

Experimental Study on Compaction Deformation and Gas Permeability Properties for Crushed Limestone

Xiaojun Yang, Zhen Li,* Hongwei Wang, Peng Yang, Yirui Yu, Zhen Tian, and Yiming Liu

Cite This: *ACS Omega* 2024, 9, 2830–2840

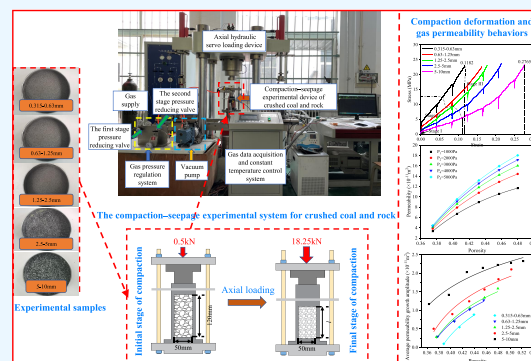
Read Online

ACCESS |

Metrics & More

Article Recommendations

ABSTRACT: The mining goaf is enriched in coalbed methane (CBM) resources, and it is imperative to realize its efficient extraction. The gas permeability properties of the crushed coal and rock in the caved zone of mining goaf are the basis for the study of its internal CBM migration and enrichment law. In this study, the compaction deformation and gas permeability properties of crushed limestone with different particle sizes were revealed. The results show that (1) the deformation resistance capacity of the crushed limestone increased with increasing stress. The decreasing trend of porosity of samples with different particle sizes in the early and later compression periods is significantly different. Particle RR of the lower layer is smaller than that of the other layers. (2) The permeability of the sample decreases with decreasing porosity and nitrogen pressure, and it is between 10^{-12} and 10^{-10} m². Nitrogen migration within the crushed limestone requires the pseudo-threshold pressure gradient, which ranges from 64.86 to 311.42 Pa/m. (3) The average permeability growth amplitude of the sample shows a logarithmic decreasing trend with the decrease of porosity. The average permeability growth amplitude of the 5–10 mm sample at the same porosity was 15.9–22.3 times that of the 0.315–0.63 mm sample. (4) The permeability of crushed limestone on both sides of the lower layer in the caved zone is much larger than that of other locations. The results are of great practical significance for accurately predicting the CBM enrichment area of mining goaf and then selecting the final position of the extraction drilling hole.



1. INTRODUCTION

China's coal resources account for about 94% of the proven fossil energy reserves and have an irreplaceable position in the energy system.^{1,2} As a clean and high-quality energy source associated with coal resources, the development and utilization of coalbed methane (CBM) have great market prospects.³ Meanwhile, it is an important direction for the development of clean energy in the future.^{4,5} CBM is abundant in the mining goaf, and realizing its efficient exploitation and utilization is of great significance to optimize the energy structure.⁶ The gas permeability properties of coal and rock media in mining goaf are the basis for studying CBM enrichment and migration and the selection of surface drilling location.^{7,8} The goaf formed by longwall mining can be divided sequentially into a caved zone, a fractured zone, and a continuous bending zone.^{9,10} Notably, the crushed coal and rock in the caved zone is a triple pore structure with pores, fractures, and voids, which means that its internal pore space is much larger than the dual pore-fracture structure in the fractured zone and continuous bending zone.¹¹ Crushed limestone is a common rock in the caved zone; it is of great theoretical and practical significance to master the evolution of its permeability properties during compaction for the efficient extraction of CBM in goaf.

As a kind of granular material, the compaction deformation behaviors of crushed coal and rock under stress will inevitably affect its permeability properties.¹² Thus, more and more researchers have paid more attention to the compaction deformation of crushed coal and rock. For crushed coal and rock, many studies have been conducted to understand the factors affecting deformation behavior such as loading rates,¹³ particle gradations, and confining pressures¹⁴ through repetitive triaxial compression experiments. Huang et al.¹⁵ and Liang et al.¹⁶ found that the compaction deformation of crushed gangue demonstrated approximately linear, nonlinear, and stable linear growth stages. In addition to this, the influence of particle crushing on macrodeformation resistance under the cyclic loading stress path was analyzed.¹⁷ Zhang et al.¹⁸ and Han et al.¹⁹ investigated the influence of lithology and compaction stress on particle crushing of crushed samples.

Received: October 17, 2023
Revised: November 14, 2023
Accepted: December 12, 2023
Published: January 4, 2024



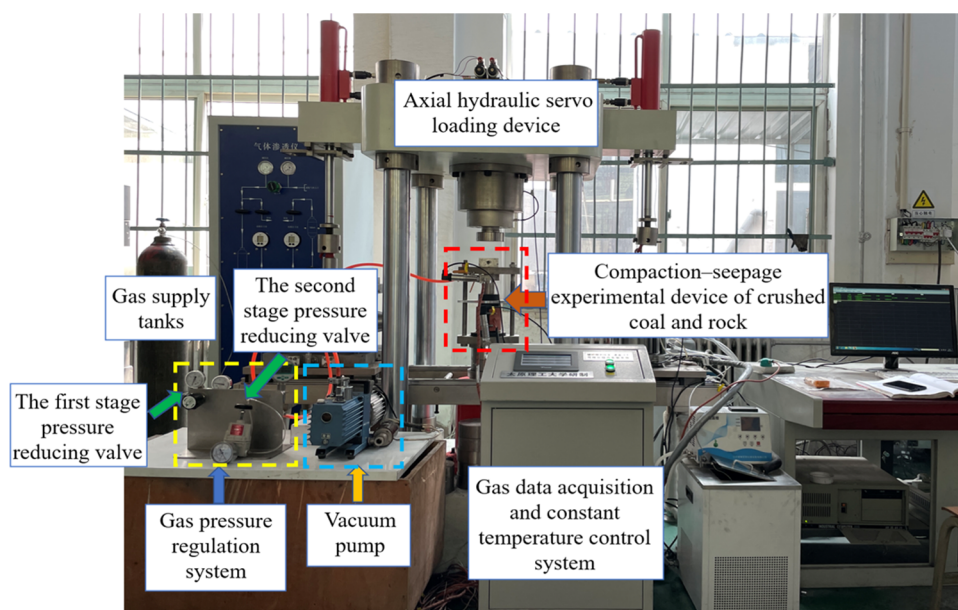


Figure 1. Compaction–seepage experimental system for crushed coal and rock.

After proposing a compaction-acoustic emission three-dimensional localization method²⁰ specifically applicable to crushed granular media, Li et al.^{21,22} investigated the macroscopic compaction deformation and the spatial and temporal evolution laws of the internal particle recrushing behaviors for crushed anthracite and gangue with different particle sizes. Through axial compression tests, many scholars have revealed that the particle refragmentation rate is positively correlated with the initial measured pressure,²³ coal–rock mixing ratio,²⁴ and the particle gradation.²⁵ The above research has laid a solid foundation for analyzing the permeability properties of crushed coal and rock.

Compared with traditional porous and fractured coal and rock, the seepage channel of crushed coal and rock is composed of a triple void structure of pores, fractures, and voids, which is much larger than that of porous and fractured coal and rock.^{26,27} Moreover, due to the influence of the overlying strata, the overall porosity and particle size of the crushed coal and rock inside the caved zone of the mining goaf are very different from those of the conventional intact crushed coal rock.²⁸ This leads to the change of porosity and particle size of crushed coal, and rock media will greatly affect the size of the permeability in the caved zone.²⁹ Early in the 21st century, many researchers carried out studies on the permeability characteristics of crushed coal and rock under the medium of water. Huang et al.³⁰ and Li et al.³¹ found that the seepage behavior of water inside crushed sandstone conforms to the nonlinear permeability law. Subsequently, it was discovered that increasing stress and decreasing particle size will lead to a decrease in the permeability of crushed sandstone.^{32,33} In recent years, the gas permeability properties of crushed coal and rock inside the mining goaf have received extensive attention as the study progressed. The effects of compaction, expansion, and seepage characteristics of natural and saturated crushed rocks were investigated.³⁴ On this basis, it was obtained that the relationship between permeability, non-Darcy coefficient, and porosity of crushed sample can be fitted using an exponential function.³⁵ Gas permeability experiments with different stress carried out on crushed coal

and rock were used to construct a stress-permeability fitting model by varying the stress conditions and the number of cycles of loading and unloading.^{36,37} Under constant total stress, permeability to sorption gas increases with a decrease of pressure due to crushed coal and rock swelling^{38,39} and decreases with increasing pressure due to matrix shrinkage.^{40,41} Pang et al. and Zhang et al.^{42,43} studied the permeability evolution of crushed coal with different porosities and found that porosity is the main factor determining the permeability of crushed coal samples.

In the above studies, the permeability of the fluid mostly occurs under the condition of a high Reynolds number. Hence, the seepage process can be well described by the non-Darcy's Forchheimer's equation. The continuous extraction inside the mining goaf will lead to the reduction of the flow rate and pressure of CBM. Subsequently, the migration of CBM in crushed coal and rock of the caved zone will be dominated by the low Reynolds number.^{29,44} The current research on the gas permeability law under the low Reynolds number of crushed coal and rock is not in-depth. Moreover, strong adsorption and desorption between the crushed coal, rock, and methane will make the internal seepage channel expand and contract, which will lead to a large difference in the permeability law.

Therefore, our group developed the first generation of compaction–permeability experimental equipment for crushed coal and rock. The relationship between the porosity, permeability, and pressure gradient of the crushed anthracite with single particle size under the low flow velocity was studied.⁴⁵ On this basis, the second-generation experimental system of compaction–seepage of crushed coal and rock was designed. This study carries out the experimental system to explore the compaction deformation and gas permeability properties of crushed limestone with different particle sizes. The results are of great practical significance for accurately mastering bearing and seepage behavior in the caved zone, predicting the CBM enrichment area of mining goaf, and then selecting the final position of the extraction drilling hole.

2. EXPERIMENTAL DESIGN

2.1. Experimental System. Figure 1 shows the second-generation experimental system of compaction–seepage of crushed coal and rock, which included a compaction–seepage experimental device of crushed coal and rock, an axial hydraulic servo loading device, gas supply tanks, a gas pressure regulation system, gas piping, a vacuum pump, gas data acquisition, and a constant temperature control system.

The gas pressure regulation system realizes the stable control of the inlet pressure by connecting two pressure reducing valves in series. The maximum inlet pressure of the first-stage pressure reducing valve was 15 MPa, and the regulating range was 0–120 kPa; the maximum inlet pressure of the second-stage pressure reducing valve was 1 MPa, and the regulating range was 0–14 kPa. The gas data acquisition system was used to monitor the following parameters in real time: inlet and outlet line temperature and pressure, gas flow, and tank temperature. Its sampling frequency was 12.5 times/s; the flow sensor measurement range was 0–2 L/min with an error of 0.2%; the pressure sensor measurement range was 0–5 kPa with an error of 0.2%. The constant temperature control system was used to maintain a constant temperature flow of gas. The outer walls of the compaction–seepage experimental device of crushed coal and rock and gas piping are fully wrapped with heating pads. Temperature sensors are installed between the heating pads, the gas piping, and the outer wall of the compaction–seepage experimental device. On this basis, the constant temperature control system will automatically determine whether heating is required according to the difference between the preset temperature and the real-time ambient temperature in order to ensure the constant temperature flow of gas medium during the whole testing process.

Figure 2 shows the compaction–seepage experimental device of crushed coal and rock, which includes a loading

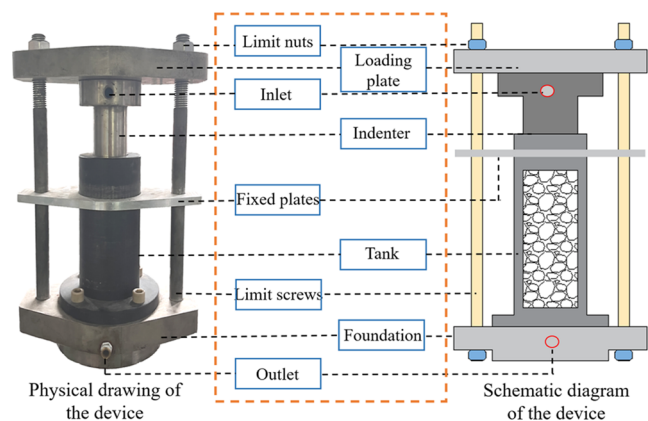


Figure 2. Compaction–seepage experimental device of crushed coal and rock.

plate, an indenter, fixed plates, a tank, an inlet, an outlet, limit nuts, limit screws, and a foundation. A loading plate is used to deliver the axial loading stress from the axial hydraulic servo loading device. This device rivets the loading plate to the indenter as a single unit to achieve better transfer of axial stress. The crushed coal and rock compaction–seepage experimental device is used to accommodate crushed limestone samples, and its charging height and internal diameters are 0.19 and 0.05 m, respectively. At the same time, its

maximum axial loading capacity is 50 kN. Fixed plates constrain the downward path of the loading plate and indenter, which prevents damage to the device caused by eccentric compression. A combination of limit screws and limit nuts was used to maintain axial displacement during seepage experiments.

2.2. Experimental Samples. The limestone material was obtained from Yanshi City, Henan Province, China. It was found that the crushed rock with a particle size of 0.05 m or less accounted for about 15–86% after blasting in the excavation face.⁴⁶ There are about 1.28–17% of brittle rock particles with size below 2 mm after the dynamic impact test.⁴⁷ The smaller the particle size, the lower the permeability of the crushed coal and rock. In the late stage of CBM extraction, this becomes the key to constrain the CBM migration properties and the efficiency of extraction in mining goaf.²⁹ Therefore, the limestone material was crushed and screened into 0.315–0.63, 0.63–1.25, 1.25–2.5, 2.5–5, and 5–10 mm samples. A standard sand screen according to GB/T 6003.1-2012 was used for screening.²⁸ The uniaxial compressive strength and density of the samples were 129 MPa and 2834 kg/m³, respectively. Figure 3 shows the diagram of these experimental samples.

2.3. Experimental Methodology. The experimental procedure of the experiment is shown below:

- (1) Sample charging. The crushed limestone samples were weighed and uniformly put into the crushed coal rock body compaction–seepage experimental device using the method described by Li et al.²² The final charging height was 120 mm.
- (2) Preloading. The rate of preloading was 0.01 kN/s. When the pressure reaches 0.5 kN, the loading was stopped and the axial displacement of the press was kept constant.
- (3) Vacuum pumping and preheating. After connecting the compaction–seepage experimental system. The sample was continuously vacuumed for more than 12 h to discharge impurity gas. Then, the tank and gas piping were heated until they reached 30 °C.
- (4) Seepage tests. The gas pressure was brought to a preset value by the gas pressure regulation system and then open the inlet and outlet valves in turn. Real-time nitrogen pressure and flow variation were collected using the data acquisition system. When the differential pressure variation was less than 3 Pa and the flow variation was less than 1 mL/min within half an hour, the first group of seepage test was ended. Changing nitrogen pressure by the gas pressure regulation system until six seepage variation tests was completed.
- (5) Axial loading. The axial loading rate was 0.01 mm/s until the loading height reached 5 mm. Step 4 is repeated until the loading stress reaches 45 kN (prevent the tank from being damaged).
- (6) Repetition of steps (1)–(5) until all compaction–seepage experiments for the five particle sizes were completed.

The porosity φ of each axial displacement level can be calculated as follows²⁹

$$\varphi = \frac{V_S - V_L}{V_S} = 1 - \frac{m}{\rho_s \cdot A \cdot (L - \chi)} \quad (1)$$



Figure 3. Experimental sample diagram.

where V_S is the total volume, V_L is the volume of the crushed coal and rock matrix, χ is the axial displacement, m is the mass of the crushed coal, ρ_s is the true density, A is the cross-sectional area of the tank, and L is the initial height of samples. In this study, $\rho_s = 2833 \text{ kg/m}^3$, $A = 0.00196 \text{ m}^2$, and $L = 0.12 \text{ m}$. In addition, the porosity is a constant parameter when axial displacement is kept steady during the experiment.

The cleat network of intact coal and rock provides seepage channels for fluid flow.^{48,49} Therefore, its permeability depends mainly on the connectivity of the cleat network, mineral composition, and lithotype of sample.⁵⁰ The studies^{29,34} show that compared to the intact coal and rock, the crushed coal and rock is a nonconsolidated porous material and its main seepage channel is the pore space between particles. Therefore, the influencing factors of permeability properties of crushed coal and rock are significantly different from those of intact coal and rock. The Reynolds number Re ⁵¹ is often used to determine the seepage behavior of viscous fluid. It is calculated as follows

$$Re = \frac{\rho \cdot v \cdot d}{\varphi \cdot \mu} \quad (2)$$

where ρ , v , and μ are the density, velocity, and dynamic viscosity coefficient of fluid media, respectively; and d is the average diameter of sample particles. In this study, $\rho = 1.25 \text{ kg/m}^3$ and $\mu = 0.18 \times 10^{-4} \text{ Pa}\cdot\text{s}$ (30 °C).

The values of Re in this study were calculated to range from 0.04 to 7.14 and to fall into the applicable range of Darcy's law. Darcy's law can be used to express the permeability k ¹²

$$k = \frac{2Q\mu LP_2}{A \cdot (P_1^2 - P_2^2)} \quad (3)$$

where Q is the nitrogen flow velocity (m^3/s), P_1 is the inlet pressure of nitrogen (Pa), and P_2 is the outlet pressure of nitrogen (Pa).

3. RESULTS AND DISCUSSION

3.1. Evolution of Macrocompaction Behavior. Crushed limestone is a granular material with no consolidation force. Different from the intact and fractured rock, the axial deformation of crushed samples under stress is much greater than that of the intact and fractured rock.⁵² Strain can be calculated as follows²⁸

$$\varepsilon = \frac{\Delta h}{h_0} \quad (4)$$

where h_0 is the initial height of the crushed limestone and Δh is the compression displacement.

In this study, it is necessary to keep the axial displacement constant in order to carry out the gas permeation test when the sample was compressed every 5 mm. Therefore, there will be a

periodic stress drop in the stress–strain curves,³⁶ as shown in Figure 4.

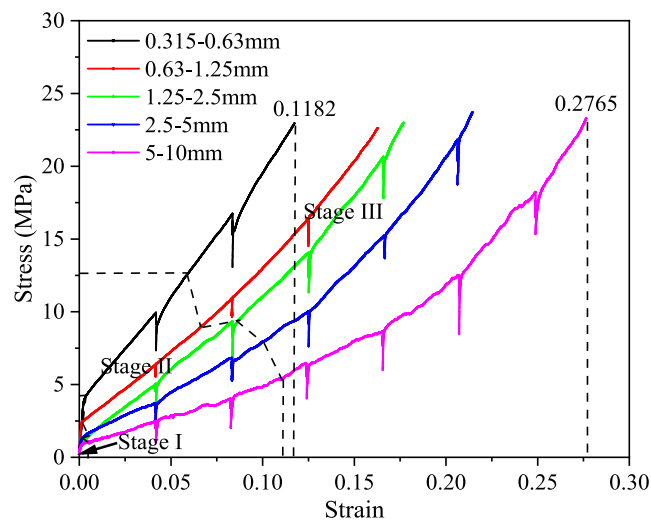


Figure 4. Stress–strain curves of crushed limestone under different particle sizes.

As can be seen from Figure 4, the stress–strain curves of crushed limestone with different particle sizes had roughly the same growth trend during compaction. According to the different tangent moduli of the curves, they were divided into initial compaction (stage I), linear compaction (stage II), and plastic compaction (stage III). The detailed classification basis for each stage is summarized in Table 1.

Table 1. Tangent Modulus Range of Different Particle Sizes of Broken Limestone at Different Deformation Stages^a

particle size (mm)	the tangent modulus range of each stage		
	stage I	stage II	stage III
0.315–0.63	–168.97	168.97–169.85	169.85–
0.63–1.25	–138.76	138.76–139.26	139.26–
1.25–2.5	–127.58	127.58–128.36	128.36–
2.5–5	–85.98	85.98–86.84	86.84–
5–10	–57.56	57.56–58.37	58.37–

^aNote: the tangent modulus range in stage I only shows the final strain point, and stage III only shows the initial strain point.

- (1) Stage I. The curves exhibited an obvious nonlinear “upward convex” growth trend, which is basically consistent with the research results of Feng et al.²¹ and Li et al.²² Moreover, the loading rate also affects the growth trend of the curves.⁵³ In this study, the loading

rate was relatively high, so the “upward convex” magnitudes of the curves were larger.

- (2) Stage II. At this stage, the tangent modulus of the curve tended to a fixed value. And the value decreased with increasing particle size. This is because large particles have a looser skeletal structure during the initial charging state, which results in a weaker deformation resistance capacity of larger particles compared to that of small particles. Therefore, the larger the particle size, the smaller the stress required to be compressed for the same height.
- (3) Stage III. The curves showed a “downward convex” growth trend. At this stage, the deformation resistance capacity of crushed limestone gradually increased. Meanwhile, the smaller the particle size, the faster its resistance to deformation grows.²¹

As shown in Figure 4, the strain of crushed limestone increased with the increase of particle size under the same stress. The maximum strain (the final strain at the peak stress) of the 0.315–0.63 mm samples was 11.82%, while that of the 5–10 mm samples was 27.65%. This is because the compactness²² of the small particle was higher than that of the large particle under the same stress. Compared to large particles, small particles are more likely to form a dense skeleton structure, which sustains stress uniformly.

In addition, compared with crushed anthracite²¹ and crushed coal gangue,²² crushed limestone with the same particle size has greater uniaxial compressive strength and stronger deformation resistance. Therefore, greater stress is needed when compressed to the same deformation stage.

The porosity is an important parameter of the physical, mechanical, and permeable properties of coal and rock.⁶ Consequently, it is of great engineering value to study the evolution of porosity in bearings of crushed coal and rock. Figure 5 shows the porosity–axial stress curves under different particle sizes. Notably, the exponential function can well represent the trend of porosity with stress, and the correlation coefficient (R^2) values for each curve exceeded 0.97

$$\varphi = a \cdot e^{b \cdot \sigma} \quad (5)$$

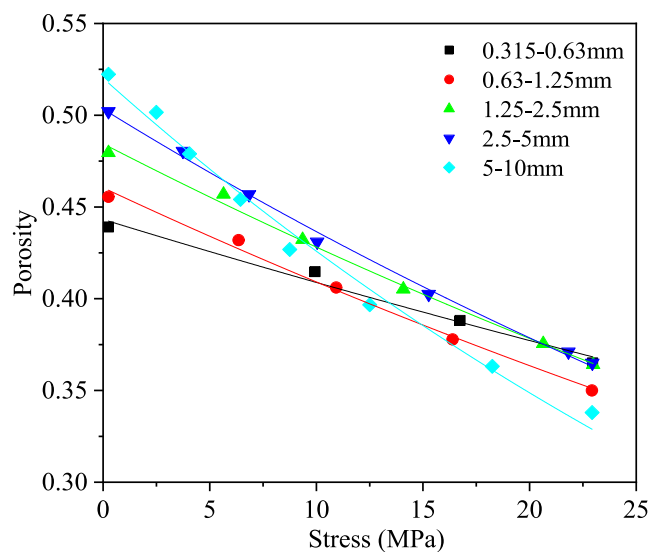


Figure 5. Porosity–axial stress curves under different particle sizes.

As shown, the porosity decreased with increasing axial stress, and the decreasing rate became progressively smaller. At the beginning of loading, the internal structure of crushed limestone was loose. The particle extrusion and slippage to fill the pore led to a sharp decrease in the porosity. The structure of the crushed limestone gradually stabilizes as the stress increases, which leads to a decrease in the rate of porosity reduction. Moreover, the porosity of large particles was larger than that of small particles in the early stage. With the increase of stress, the porosity of large particles decreased rapidly and was gradually smaller than that of small particles.

Li et al.²⁹ found that crushed coal and rock in the caved zone will appear as a layered recrushing phenomenon under overburden pressure in 2018. Subsequently, Feng et al.²⁸ proposed that the particle recrushing rate (RR) for the first time provided a new quantitative method for characterizing the particle recrushing of crushed coal and rock. Based on this, Li et al.²² concluded that there exists inhomogeneous deformation and layered recrushing properties in bearing crushed coal gangue. In this study, to further explore and verify the layered recrushing behavior of crushed limestone, the particles in the final compression state were layered and screened, and the dichotomy method was used for the statistical analysis. Figure 6 shows the evolution of the particle RR of crushed limestone with different particle sizes in the final compression state.

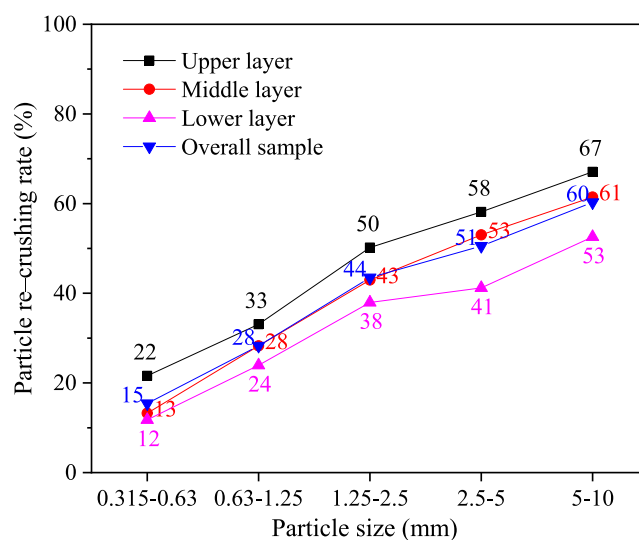


Figure 6. Particle recrushing rate in the final compression state.

As shown, the evolution of particle RR in each layer shows the same trend for crushed limestone with different particle sizes, that is, upper layer > middle layer > lower layer, which is similar to bearing crushed coal gangue.²² This is because the axial stress first acts on top of the samples and then transfers from the top to lower sections, and this process is nonuniform. The upper layer near the force application end has a denser skeleton structure, which is conducive to the occurrence of particle recrushing events. Therefore, the particle RR of the upper layer is higher than that of other layers. At the same time, the particle RR of the overall sample is basically the same as that of the middle layer. This is because the distance between the middle layer and the force application end has a smaller impact on the different force chain transmission effects compared with that of the upper and lower layers. This results

in a similar particle RR between the overall sample and middle layer.

The particle RR significantly increases with the increase in particle size. The overall particle RR rate of 5–10 mm sample reaches 60%, which is 4 times higher than that of the 0.315–0.63 mm sample. In the meantime, compared with the 0.315–0.63 mm sample, the particle RR of the upper, middle, and lower layers of the 5–10 mm sample increased by 45, 48, and 41%, respectively. This indicates that smaller particles have stronger bearing capacity than larger ones, which are more difficult to recrush.

In addition, the quantitative analysis results of particle size in each layer of crushed anthracite under different stresses by CT scanning and reconstruction can also prove this point.⁵⁴ These results further illustrate the particle distribution of crushed coal and rock in the caved zone; that is, the overall particles of the lower layer are the largest, followed by the middle layer, and that of the upper layer are the smallest. In summary, it can be seen that the porosity of the lower layer is much larger than that of the middle and upper layers in the caved zone. This results in the lower layer of the caved zone being easier for CBM migration and enrichment.

3.2. Gas Permeability Properties of Crushed Limestone. **3.2.1. Variation of Flow Velocity with Gas Pressure Gradients.** As stated in Section 1, Forchheimer's equation is often used to describe the high-velocity non-Darcy flow of CBM in the early stage of extraction.⁵⁵ However, the gas pressure gradually decreases to a lower level in the actual extraction process.⁴⁴ Therefore, a lower gas pressure was chosen for testing in this study.

In this paper, the evolution law of the internal flow velocity with the gas pressure gradient was analyzed by taking 1.25–2.5 mm crushed limestone samples as an example. Figure 7

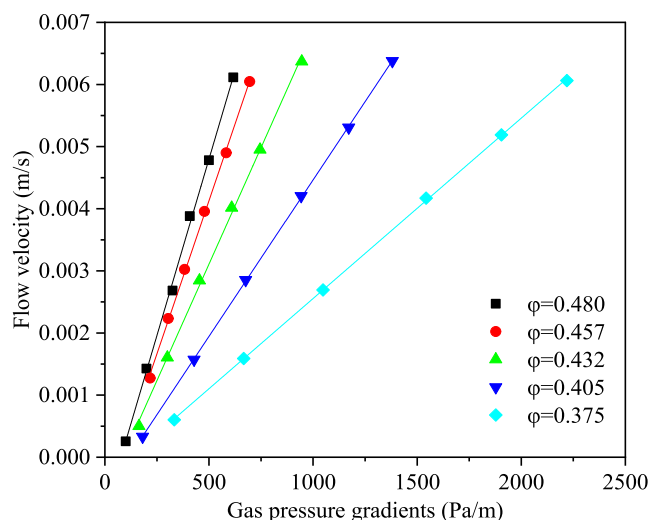


Figure 7. Flow velocity vs gas pressure gradient curves for the 1.25–2.5 mm crushed limestone.

illustrates the flow velocity versus gas pressure gradient curves for the 1.25–2.5 mm crushed limestone. Apparently, the relationship between the flow velocity and gas pressure gradient can be well represented by a linear function under lower gas pressure. This further demonstrates that the application of the Darcy law can better characterize the seepage of the crushed limestone in this study. The slopes of the curves increased with increasing porosity. This indicated

that crushed limestone with larger porosity was more sensitive to the variation of gas pressure gradients.

Notably, the fitted curves did not pass through the origin of the coordinates, which was similar to the non-Darcy flow curve for low-permeability rocks. This indicated that nitrogen migration within the crushed limestone under low-velocity seepage conditions requires the threshold pressure gradient.^{29,45}

Figure 8 shows the relationship between the parameters of the flow velocity–pressure gradient fitting curve and porosity.

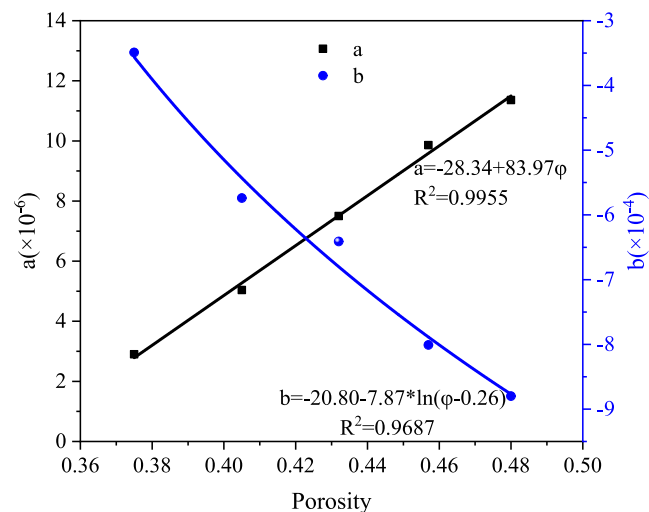


Figure 8. Relationship between parameters of flow velocity–pressure gradient fitting curve and porosity.

As shown, the value of parameter a increases linearly, while that of parameter b decreases with the increase of porosity. Further, the nitrogen migration in crushed limestone can be expressed as

$$\begin{cases} v = (-28.34 + 83.97\varphi) \cdot \frac{dP}{dL} - 20.80 & \frac{dP}{dL} > \text{TPG} \\ -7.87 \cdot \ln(\varphi - 0.26) & \\ v = 0 & \frac{dP}{dL} \leq \text{TPG} \end{cases} \quad (6)$$

From eq 6, when the gas pressure gradient is less than the pseudo-threshold pressure gradient, the flow velocity is 0. Therefore, assuming that the flow velocity is 0, and the porosity is substituted into eq 6, the pseudo-threshold pressure gradient of samples will be obtained. At $v = 0$, the pseudo-threshold pressure gradient of the 1.25 mm to 2.5 mm sample was obtained for the above five porosities, i.e., 77.46, 81.24, 85.47, 113.89, and 120.34 Pa/m. By this method, the pseudo-threshold pressure gradient for the remaining four particle sizes of crushed limestone was similarly calculated. And the pseudo-threshold pressure gradient for all samples is 64.86–311.42 Pa/m. Meanwhile, the pseudo-threshold pressure gradient for all samples shows an increasing trend with decreasing porosity. This is similar to methane exhibiting a pseudo-threshold pressure gradient of 80.87–103.05 Pa/m in crushed anthracite.⁴⁵ However, Wei et al.⁵⁶ found that the proposed initiation pressure gradient for low-permeability rocks is 0–1000 Pa/m. The reason for this difference may be the different magnitudes of the main seepage channels. The seepage

channels of crushed limestone are mainly millimeter- and micrometer-scale voids between particles, which are far more than the micrometer- and nanometer-scale pores and cracks in the low-permeability rocks. And the pseudo-threshold pressure gradient increases with the decrease of seepage channels. Moreover, this also leads to an increase in the pseudo-threshold pressure gradient with decreasing porosity.

3.2.2. Evolution of Permeability with Gas Pressure and Porosity. Shi and Durucan⁵⁷ observed the continuous exponential growth behaviors of coalbed permeability with reservoir pressure depletion and attributed this phenomenon to the Klinkenberg effect and internal swelling induced by methane sorption. Meanwhile, it is worth noting that the permeability increases logarithmically with an increase of the inlet pressure in this study, as shown in Figure 9.

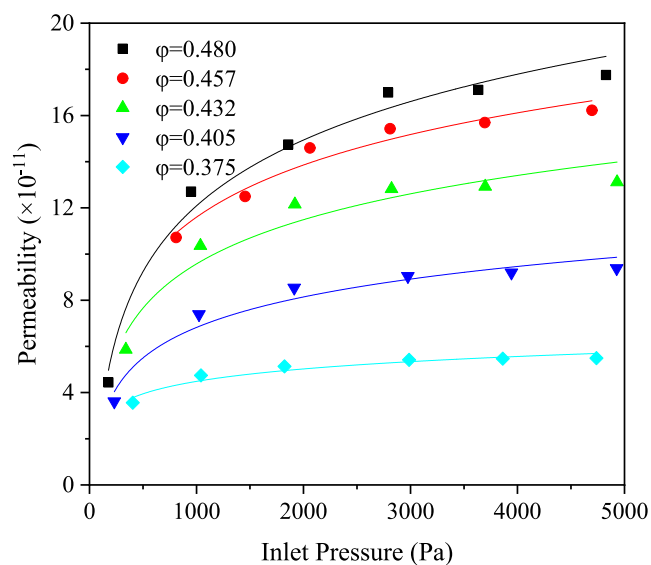


Figure 9. Relation curve of the crushed limestone permeability and inlet pressure.

As shown, the growth tendencies of the curves were homologous. The permeability shows an apparent growth with an increasing nitrogen pressure. This is consistent with the trend of permeability with methane pressure in crushed coal.⁴⁵ Notably, the following trend of the logarithmic function is proposed to fit the relationship

$$k = a \cdot \ln P_1 + b \quad (7)$$

The logarithmic function relationship is the result of a combination of two effects. On the one hand, the average main seepage channels become smaller due to larger swelling deformation induced by larger nitrogen pressure. On the other hand, the molecular mean free path becomes smaller as nitrogen pressure increases. The above two reasons cause the difficulty of nitrogen migration within the crushed limestone to increase with increasing pressure. Consequently, the permeability increasing rate becomes smaller with an increasing nitrogen pressure.

Moreover, the high value of the correlation coefficient (R^2) for each curve indicates a good fit. Figure 10 illustrates the regression analysis between porosity and fitted parameters of a and b to investigate the relationship between the three. As can be seen, the value of parameter a increases, while that of b decreases with the increase in porosity. Further, we can obtain

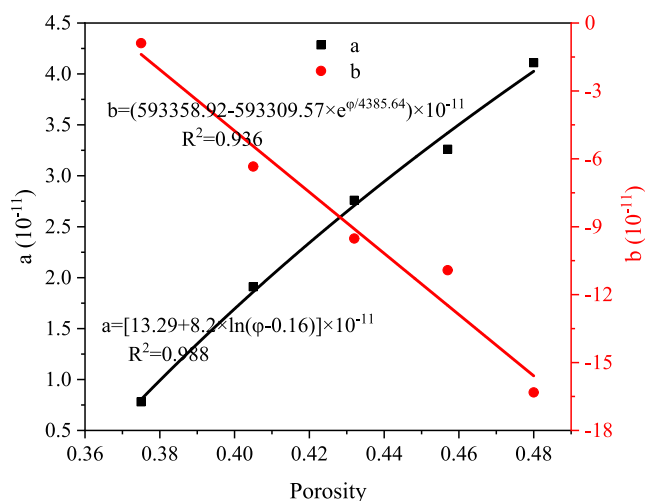


Figure 10. Permeability–inlet pressure fitting curve parameters and porosity.

the common relationships among the permeability, porosity, and nitrogen pressure for crushed limestone as

$$k = \left[[13.29 + 8.2 \cdot \ln(\varphi - 0.16)] \cdot \ln P_1 + (593358.92 - 593309.57 \cdot e^{(\varphi/4385.64)}) \right] \times 10^{-11} \quad (8)$$

From eq 8, it can be further shown that the permeability was not sensitive to the change of porosity when the nitrogen pressure was certain. To further study the effect of the porosity variation on permeability, the permeability versus porosity under various inlet pressures based on eq 8 was obtained, as shown in Figure 11.

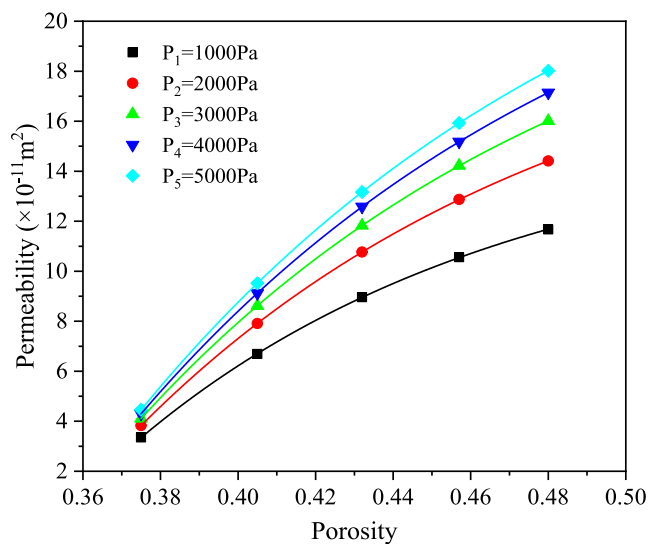


Figure 11. Evolution curve of permeability with porosity under different gas pressures.

As shown, the curves show a similar growth trend: permeability decreased exponentially with decreasing porosity, and the decreasing rate became progressively larger. This is because the seepage channels within the crushed limestone decreased with decreasing porosity, which made nitrogen migration increasingly difficult. And the more developed pore

structure can make the permeability decrease by a larger degree with greater porosity when the porosity decreases by the same degree.

Moreover, the permeability was more sensitive to porosity variation under a larger gas pressure. The reason may be that the continuum Darcy flow turns into slip flow in the later stage due to the lower flow velocity and nitrogen pressure. The slip effect facilitates the migration of gas molecules on the tube wall, and the velocity is no longer zero, thus providing an additional flow velocity that makes the measured permeability higher than the actual permeability. Hence, the permeability experiences greater changes when the porosity decreases by the same degree under a higher nitrogen pressure.

3.2.3. Evolution of Permeability with Particle Size. The tortuosity of crushed coal and rock increases with decreasing particle size, which forms a longer seepage channel.⁵⁸ As a result, the particle size of crushed limestone likewise affects the evolution of permeability. In this paper, the permeability of the specimen under different gas pressure points in each compression stage was obtained on the basis of eq 8. On this basis, the average permeability growth amplitude⁵⁹ was calculated to homogenize the permeability at different pressure points, which was used to reveal the effect of particle size on permeability. The average permeability growth amplitude is calculated as follows

$$\Delta k = k_{i+1} - k_i \quad (i = 1, 2, \dots, 4) \quad (9)$$

$$\Delta \bar{k} = \frac{1}{n} \cdot \sum_{j=1}^n \Delta k_j \quad (10)$$

where Δk is the permeability growth amplitude, m^2 ; k_{i+1} is the permeability of the crushed limestone at the $i + 1$ first gas pressure point, m^2 ; $\Delta \bar{k}$ is the average permeability growth amplitude, m^2 ; and Δk_j is the j th permeability growth amplitude, m^2 .

The average permeability growth amplitude of crushed limestone with porosity evolution for different particle sizes is presented in Figure 12. As shown, the average permeability growth amplitudes of different particle sizes increase logarithmically with increasing porosity

$$\Delta \bar{k} = \ln(a + b \cdot \varphi) \quad (11)$$

This is because the adsorption of gas on the surface of particles will lead to a decrease in permeability. The fitted parameters for different particle sizes are summarized in Table 2, where the high value of coefficient determination (R^2) for each curve in this table is an indication of good fitting. As can be seen, the value of parameter a decreases, while that of parameter b increases with the increase of particle size.

From the fitted curves, it can be seen that the average permeability growth amplitude of 5–10 mm samples at the same porosity was 15.9–22.3 times that of 0.315–0.63 mm. It shows that the permeability of the sample increases with the increase of particle size, which is similar to the findings of Miao et al.⁵⁵ Moreover, for smaller particles, the slope of the curve was greater for the same porosity. This indicates that the decrease in porosity has a more significant effect on the permeability of samples with a smaller particle size. The seepage channel within the crushed limestone decreases with the decrease of the particle size under the same porosity. Consequently, the decrease in the permeability caused by adsorption will be more significant for the small particles,

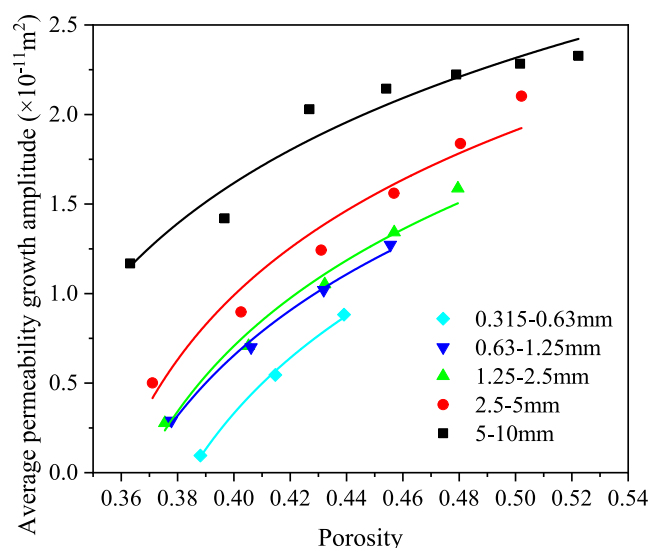


Figure 12. Evolution of the average permeable growth amplitude with porosity under different particle sizes.

Table 2. Parameters of the Average Permeability Growth Amplitude and Porosity Fitting Curve

particle size (mm)	a	b	R^2
0.315–0.63	−8.70	25.24	0.995
0.63–1.25	−9.09	27.54	0.992
1.25–2.5	−10.41	31.08	0.978
2.5–5	−13.59	40.70	0.945
5–10	−15.34	50.95	0.928

which have relatively small seepage channels. This phenomenon also indicates that the influence of particle size variation on permeability cannot be ignored during the practice of CBM extraction.

By calculation, it can be found that the permeability of bearing crushed limestone samples ranged from 10^{-12} to 10^{-10} m^2 , which is much greater than that of the intact and fractured coal and rock. This is because the main seepage channel of crushed limestone should be a millimeter-scale pore, whose scale is more than 1–2 orders of magnitude larger than the nanopore and micrometer cleats of the main seepage channel of intact coal and rock samples. Considering the larger block size of the crushed coal and rock at the project site, the CBM in the caved zone is more easily migrated. This leads to the caved zone belonging to the high-permeability area of CBM. Considering the permeability of coal and rock, the “uplift effect” of coalbed methane and its fully enclosed and nonventilated characteristics in the abandoned mining goaf, the crushed coal and rock in the caved zone together with the “high-level annular fracture body” developed by the longitudinal penetrating cracks constitute the “U”-type high-permeability CBM enrichment area in abandoned mining goaf along the strike and longitudinal section.

Moreover, in Section 3.1, we analyzed that the particle distribution of crushed coal and rock at each layer in the caved zone, in conjunction with the particles on both sides of the caved zone, is larger than that of the middle area of the caved zone.²² The conclusion that the porosity on both sides of the lower layer is greater than that of other locations in mining goaf was obtained. In summary, the gas permeability of crushed coal and rock on both sides of the lower layer in the

caved zone is much larger than that of the other locations in mining goaf. These results provide highly practical guidance for the efficient extraction of CBM from the abandoned mining goaf; i.e., greater CBM extraction efficiency may hence be realized by locating the end position of the surface borehole to the lower layer of the caved zone at both sides of mining goaf. In the practice of CBM surface extraction engineering in the abandoned goaf of the Jincheng mining area, more than 20 surface wells have achieved good extraction results by locating the final position of the surface borehole in the “U”-type high-permeability CBM enrichment area.²⁹

4. CONCLUSIONS

- (1) The macrodeformation of crushed limestone could be divided into initial compression, linear compaction, and plastic compaction stages. The deformation resistance capacity of the crushed samples increased with increasing stress. The porosity of larger particles is greater than that of smaller ones in the early compression, while the reverse is true in the later compression. Particle RR of the lower layer is smaller than that of other layers. Moreover, particle RR increases with increasing particle size.
- (2) The permeability of the crushed limestone sample is between 10^{-12} and 10^{-10} m², which is much larger than that of the intact and fractured rocks. The permeability decreases with a decreasing porosity of the sample and nitrogen pressure. Nitrogen migration within the crushed limestone under low-velocity seepage conditions requires the pseudo-threshold pressure gradient, which ranges from 64.86 to 311.42 Pa/m. Moreover, the pseudo-threshold pressure gradient decreases with an increase of porosity.
- (3) The average permeability growth amplitude of crushed limestone shows a logarithmic decreasing trend with the decrease of porosity. Particle size has a significant impact on the evolution of the average permeability growth amplitude. The average permeability growth amplitude of the 5–10 mm sample at the same porosity was 15.9–22.3 times that of the 0.315–0.63 mm sample.
- (4) In this paper, the compaction deformation and gas permeability properties of crushed limestone were systematically studied. It is found that the permeability of crushed limestone on both sides of the lower layer in the caved zone is much larger than that of other locations. Considering the enclosed and nonventilated characteristics in the abandoned mining goaf, a greater CBM extraction efficiency may hence be realized by locating the end position of the surface borehole to the lower layer of the caved zone at both sides of the abandoned mining goaf.

The influence of lithology on the permeability distribution in the caved zone should not be neglected. The next step is to expand the range of experimental objects and grain sizes. Meanwhile, future studies will consider analyzing the pore structure evolution mechanisms on gas permeability properties from a mesoscale perspective.

■ AUTHOR INFORMATION

Corresponding Author

Zhen Li – College of Safety and Emergency Management Engineering, Taiyuan University of Technology, Taiyuan

030024, China; State Key Laboratory of Green and Low-carbon Development of Tar-rich Coal in Western China, Xi'an University of Science and Technology, Xi'an 710054, China; Email: lizhen3345@163.com

Authors

Xiaojun Yang – College of Safety and Emergency Management Engineering, Taiyuan University of Technology, Taiyuan 030024, China; orcid.org/0009-0001-4645-4599

Hongwei Wang – State Key Laboratory of Green and Low-carbon Development of Tar-rich Coal in Western China, Xi'an University of Science and Technology, Xi'an 710054, China

Peng Yang – College of Safety and Emergency Management Engineering, Taiyuan University of Technology, Taiyuan 030024, China

Yirui Yu – College of Safety and Emergency Management Engineering, Taiyuan University of Technology, Taiyuan 030024, China

Zhen Tian – College of Safety and Emergency Management Engineering, Taiyuan University of Technology, Taiyuan 030024, China

Yiming Liu – College of Safety and Emergency Management Engineering, Taiyuan University of Technology, Taiyuan 030024, China

Complete contact information is available at:

<https://pubs.acs.org/10.1021/acsomega.3c08132>

Notes

The authors declare no competing financial interest.

■ ACKNOWLEDGMENTS

This research was supported by the Distinguished Youth Funds of the National Natural Science Foundation of China (No. 51925402), the National Natural Science Foundation of China (No. 51904198), the Shanxi Science and Technology Major Project (20201102004), and State Key Laboratory of Green and Low-carbon Development of Tar-rich Coal in Western China (SKLCRKF1911).

■ REFERENCES

- (1) Feng, G. R.; Zhang, Y. J.; Qi, T. Y.; Kang, L. X. Status and research progress for residual coal mining in China. *J. China Coal Soc.* **2020**, *45*, 151–159.
- (2) Li, Y.; Pan, S. Q.; Ning, S. Z.; Shao, L. Y.; Jing, Z. H.; Wang, Z. S. Coal measure metallogeny: Metallogenic system and implication for resource and environment. *Sci. China (Earth Sci.)* **2022**, *65*, 1211–1228.
- (3) Feng, L.; Paul, I. P.; Zhu, S. H.; Robert, J. P.; Liu, Y. Tropical methane emissions explain large fraction of recent changes in global atmospheric methane growth rate. *Nat. Commun.* **2022**, *13*, No. 1378.
- (4) Vedachalam, N.; Srinivasalu, S.; Rajendran, G.; Ramadass, G. A.; Atmanrand, M. A. Review of unconventional hydrocarbon resources in major energy consuming countries and efforts in realizing natural gas hydrates as a future source of energy. *J. Nat. Gas Sci. Eng.* **2015**, *26*, 163–175.
- (5) Li, Y.; Wang, Z. S.; Tang, S. H.; Elsworth, D. Re-evaluating adsorbed and free methane content in coal and its ad- and desorption processes analysis. *Chem. Eng. J.* **2022**, *428*, No. 131946.
- (6) Feng, G. R.; Hu, S. Y.; Li, Z.; Jiang, H. N.; Zhang, Y. T.; Xu, G.; Wang, Z.; Kang, L. X. Distribution of methane enrichment zone in abandoned coal mine and methane drainage by surface vertical boreholes: A case study from China. *J. Nat. Gas Sci. Eng.* **2016**, *34*, 767–778.

- (7) Guo, M. J.; Guo, W. B.; Yuan, R. P.; Zhao, G. B.; Bai, E. H.; Li, G. F. Spatial location determination of directional bore holes based on regional distribution characteristics of mining-induced overburden fractures. *J. Min. Saf. Eng.* **2022**, *39*, 817–826.
- (8) Lin, R. Y.; Jia, Y.; Sun, L. Experimental study on the seepage characteristics of multilayer commingled production and influencing factors of the development effect in low-permeability tight sandstone gas reservoirs. *ACS Omega* **2022**, *7*, 34080–34088.
- (9) Wang, Z. Q.; Li, P. F.; Wang, L.; Gao, Y.; Guo, X. F.; Chen, C. F. Method of division and engineering use of “three band” in the stope again. *J. China Coal Soc.* **2013**, *38*, 287–293.
- (10) Wang, L. C.; Xue, Y.; Chao, Z. Z.; Kong, H. L.; Han, J. Y.; Zhang, Z. Z. Experimental Study on Mode I Fracture Characteristics of Granite after Low Temperature Cooling with Liquid Nitrogen. *Water* **2023**, *15*, 3442.
- (11) Zhang, C.; Zhao, Y. X.; Tu, S. H.; Zhang, T. Numerical simulation of compaction and re-breakage characteristics of coal and rock samples in goaf. *Chin. J. Geotech. Eng.* **2020**, *42*, 696–704.
- (12) Yin, G.; Li, M.; Wang, J. G.; Xu, J.; Li, W. Mechanical behavior and permeability evolution of gas infiltrated coals during protective layer mining. *Int. J. Rock Mech. Min.* **2015**, *80*, 292–301.
- (13) Alnedawi, A.; Nepal, K. P.; Al-Ameri, R. Effect of loading frequencies on permanent deformation of unbound granular materials. *Int. J. Pavement Eng.* **2021**, *22*, 1008–1016.
- (14) Ma, D.; Zhang, J. X.; Duan, H. Y.; Huang, Y. L.; Li, M.; Sun, Q.; Zhou, N. Reutilization of gangue wastes in underground backfilling mining: Overburden aquifer protection. *Chemosphere* **2021**, *264*, No. 128400.
- (15) Huang, Y. L.; Li, J. M.; Ma, D.; Gao, H. D.; Guo, Y. C.; Ouyang, S. Y. Triaxial compression behaviour of gangue solid wastes under effects of particle size and confining pressure. *Sci. Total Environ.* **2019**, *693*, No. 133607.
- (16) Liang, B.; Liu, X. D.; Jin, J. X.; Yang, Y.; Wang, B. F.; Wu, P. F. Effect of particle size on the compression characteristics of vermiculite under three-way loading. *J. Liaoning Tech. Univ. (Nat. Sci.)* **2020**, *39*, 99–106.
- (17) Li, J. M.; Huang, Y. L.; Chen, Z. W.; Zhang, J. X.; Jiang, H. Q.; Zhang, Y. C. Characterizations of macroscopic deformation and particle crushing of crushed gangue particle material under cyclic loading: In solid backfilling coal mining. *Powder Technol.* **2019**, *343*, 159–169.
- (18) Zhang, J. W.; Wang, H. L.; Chen, S. J.; Li, Y. L. Characteristics of pressurized deformation of large-size crushed rock. *J. China Coal Soc.* **2018**, *43*, 1000–1007.
- (19) Han, H. Q.; Chen, S. S.; Fu, H.; Zheng, C. F. Particle breakage of rockfill materials under cyclic loadings. *Chin. J. Geotech. Eng.* **2017**, *39*, 1753–1760.
- (20) Li, Z.; Shen, X.; Feng, G. R.; Li, J. Z.; Jiang, H. N.; Song, C.; Cui, J. Q.; Niu, X. H.; Zhang, C. W.; Pei, X. M.; Wei, H. R. An Experimental Device and Method for Compaction, Acoustic Emission and Resistivity of Broken Coal and Rock Mass. Chinese Patent CN109855967A, 2019.
- (21) Feng, G. R.; Fang, Z. L.; Li, Z.; Qi, T. Y.; Zhao, J. P.; Fan, W. C.; Yang, P.; Yang, X. J.; Yu, Y. R.; Zhang, H. F.; Wang, Z. W. Effect of particle size on re-crushing characteristics of crushed coal during axial loading. *Powder Technol.* **2022**, *407*, No. 117675, DOI: 10.1016/j.powtec.2022.117675.
- (22) Li, Z.; Yang, X. J.; Yang, P.; Feng, G. R.; Liu, J. Y.; Zhu, C. Q.; Cheng, X. Layered re-breaking behavior of gangue backfilling materials and inspirations for protecting mined ecological environments. *Constr. Build. Mater.* **2023**, *368*, No. 130477.
- (23) Xin, Y. J.; Hao, H. C.; Lu, X.; Ji, H. Y.; An, D. C. Compaction characteristics test of broken rock in initial lateral pressure. *J. China Coal Soc.* **2018**, *43*, 457–465.
- (24) Tang, J. X.; Wang, Y. L.; Wang, Y. L.; Dai, Z. Y.; Li, C. Bearing Characteristics of Broken Coal and Rock under Constraint Compression Condition. *Chin. J. Underground Space Eng.* **2021**, *17*, 1399–1407.
- (25) Zhang, T. J.; Liu, N.; Pang, M. K.; Zhang, X. F.; Guo, Y.; Zhang, S. Re-crushing characteristics in the compaction process of graded crushed coal rock mass. *J. Min. Saf. Eng.* **2021**, *38*, 380–387.
- (26) Hu, S. Y.; Li, Z.; Feng, G. R.; Xu, G.; Xia, T. Q.; Jiang, H. N.; Zhang, Y. T.; Cheng, J. W.; Gao, Q.; Wang, Z.; Zhang, J. L. Changes on methane concentration after CO₂ injection in a longwall gob: A case study. *J. Nat. Gas Sci. Eng.* **2016**, *29*, 550–558.
- (27) Li, Y.; Yang, J. H.; Pan, Z.; Tong, W. S. Nanoscale pore structure and mechanical property analysis of coal: An insight combining AFM and SEM images. *Fuel* **2020**, *260*, No. 116352.
- (28) Feng, G. R.; Zhao, J. P.; Wang, H. W.; Li, Z.; Fang, Z. L.; Fan, W. C.; Yang, P.; Yang, X. J. Study of the internal re-breaking characteristics of broken limestone during compression. *Powder Technol.* **2022**, *396*, 449–455.
- (29) Li, Z. *Research on the Deformation and Seepage Characteristics of Crushed Coal and Rock and its Application in Abandoned Coal Mine Methane Extraction* Taiyuan University of Technology: 2018.
- (30) Huang, X. W.; Tang, P.; Miao, X. X.; Chen, Z. Q. Testing study on seepage properties of broken sandstone. *Rock Soil Mech.* **2005**, *26*, 1385–1388.
- (31) Li, S. C.; Miao, X. X.; Chen, Z. Q.; Mao, X. B. Experimental study on seepage properties of non-Darcy flow in confined broken rocks. *Eng. Mech.* **2008**, *25*, 85–91.
- (32) Miao, X. X.; Li, S. C.; Chen, Z. Q.; Liu, W. Q. Experimental Study of Seepage Properties of Broken Sandstone Under Different Porosities. *Transp. Porous Media* **2010**, *86*, 805–814, DOI: 10.1007/s11242-010-9653-1.
- (33) Yang, W.; Wang, S. G.; Chen, J. H. Preliminary study on laws of steady state seepage of gas in broken rock mass. *Coal Technol.* **2015**, *34*, 189–191.
- (34) Ma, D.; Bai, H. B.; Chen, Z. Q.; Pu, H. Effect of particle mixture on seepage properties of crushed mudstones. *Transp. Porous Media* **2015**, *108*, 257–277.
- (35) Ma, D.; Miao, X. X.; Wu, Y.; Bai, H. B.; Wang, J. G.; Rezaia, M.; Hang, Y. H.; Qian, H. W. Seepage properties of crushed coal particles. *J. Pet. Sci. Eng.* **2016**, *146*, 297–307.
- (36) Zhang, C.; Tu, S. H.; Zhang, L. Analysis of Broken Coal Permeability Evolution Under Cyclic Loading and Unloading Conditions by the Model Based on the Hertz Contact Deformation Principle. *Transp. Porous Media* **2017**, *119*, 739–754.
- (37) Li, B.; Zou, Q. L.; Liang, Y. P. Experimental Research into the Evolution of Permeability in a Broken Coal Mass under Cyclic Loading and Unloading Conditions. *Appl. Sci.* **2019**, *9*, 762.
- (38) Mazumder, S.; Wolf, K. H. Differential swelling and permeability change of coal in response to CO₂ injection for ECBM. *Int. J. Coal Geol.* **2008**, *74*, 123–138.
- (39) Pan, Z. J.; Connell, L. D.; Camilleri, M. Laboratory characterisation of coal reservoir permeability for primary and enhanced coalbed methane recovery. *Int. J. Coal Geol.* **2010**, *82*, 252–261.
- (40) Meng, J. Q.; Nie, B. S.; Zhao, B.; Ma, Y. C. Study on law of raw coal seepage during loading process at different gas pressures. *Int. J. Min. Sci. Technol.* **2015**, *25*, 31–35.
- (41) Meng, Y.; Li, Z. P.; Lai, F. P. Experimental study on porosity and permeability of anthracite coal under different stresses. *J. Pet. Sci. Eng.* **2015**, *133*, 810–817.
- (42) Pang, M. K.; Zhang, T. J.; Meng, Y. K.; Ling, Z. Q. Experimental study on the permeability of crushed coal medium based on the Ergun equation. *Sci. Rep.* **2021**, *11*, No. 23030, DOI: 10.1038/s41598-021-02524-4.
- (43) Pang, M. K.; Zhang, T. J.; Ji, X.; Wu, J. Y.; Song, S. Measurement of the coefficient of seepage characteristics in pore-crushed coal bodies around gas extraction boreholes. *Energy* **2022**, *254*, No. 124276.
- (44) Kong, H. L.; Chen, Z. Q.; Wang, L. Z.; Shen, H. D. Experimental study on permeability of crushed gangues during compaction. *Int. J. Miner. Process.* **2013**, *124*, 95–101.
- (45) Li, Z.; Feng, G. R.; Jiang, H. N.; Hu, S. Y.; Cui, B. Q.; Song, C.; Gao, Q.; Qi, T. Y.; Guo, X. Q.; Li, C.; Kang, L. X. The correlation

between crushed coal porosity and permeability under various methane pressure gradients a case study using Jincheng anthracite. *Greenhouse Gases: Sci. Technol.* **2018**, *8*, 493–509.

(46) Sirotyuk, G. N. A method of calculating the fragment–size composition of blasted rock from the given oversize fragment dimension. *Soviet Min. Sci.* **1970**, *6*, 59–64.

(47) Hou, T. X.; Xu, Q.; Zhou, J. W. Size distribution, morphology and fractal characteristics of brittle rock fragmentations by the impact loading effect. *Acta Mech.* **2015**, *226*, 3623–3637.

(48) Clarkson, C. R.; Bustin, R. M. Variation in micropore capacity and size distribution with composition in bituminous coal of the Western Canadian Sedimentary Basin: implications for coalbed methane potential. *Fuel* **1996**, *75*, 1483–1498, DOI: [10.1016/0016-2361\(96\)00142-1](https://doi.org/10.1016/0016-2361(96)00142-1).

(49) Wang, L. C.; Zhang, W.; Cao, Z. Z.; Xue, Y.; Liu, J. Q.; Zhou, Y.; Duan, C. Y.; Chen, T. Effect of weakening characteristics of mechanical properties of granite under the action of liquid nitrogen. *Front. Ecol. Evol.* **2023**, *11*, No. 1249617, DOI: [10.3389/fevo.2023.1249617](https://doi.org/10.3389/fevo.2023.1249617).

(50) Ramandi, H. L.; Mostaghimi, P.; Armstrong, R. T.; Saadatfar, M.; Pinczewski, W. C. Porosity and permeability characterization of coal: a micro-computed tomography study. *Int. J. Coal Geol.* **2016**, *154–155*, 57–68.

(51) Shang, H. B.; Jin, D. W.; Zhang, T. J.; Li, S. G.; Wang, Z. Z.; Zhao, C. H.; Zhou, Z. F.; Liu, Z. X. Permeability evolution of broken coal under triaxial stress. *J. China Coal Soc.* **2019**, *44*, 1066–1075.

(52) Jiang, Z. Y.; Couples, G. D.; Lewis, H.; Mangione, A. An investigation into preserving spatially-distinct pore systems in multi-component rocks using a fossiliferous limestone example. *Comput. Geosci.* **2018**, *116*, 1–11.

(53) Tang, J. X.; Zhang, Z. J.; Wang, Y. L.; Dai, Z. Y.; Kong, L. R.; Wang, Y. L.; Hou, Y. Y. Research on compressive deformation characteristics of broken rock under different loading rates. *Min. Res. Dev.* **2021**, *41*, 89–96.

(54) Feng, G. R.; Zhang, Y. D.; Li, Z.; Fang, Z. L.; Yang, Y. Q.; Yang, X. H.; Zhang, X. M. Quantitative analysis of layered re-crushing of crushed coal particles during compression based on CT scanning. *Powder Technol.* **2023**, *426*, No. 118638.

(55) Miao, X. X.; Li, S. C.; Chen, Z. Q.; Liu, W. Q. Experimental study of seepage properties of broken sandstone under different porosities. *Transp. Porous Media* **2011**, *86*, 805–814.

(56) Wei, X.; Lei, Q.; Liu, X. G.; Gao, S. S.; Hu, Z. M. Pseudo threshold pressure gradient to flow for low permeability reservoirs. *Pet. Explor. Dev.* **2009**, *36*, 232–236.

(57) Shi, J.-Q.-Q.; Durucan, S. Exponential growth in San Juan basin fruitland coalbed permeability with reservoir drawdown: Model match and new insights. *SPE Reserv. Eval Eng.* **2010**, *13*, 914–925.

(58) Yang, B.; Xu, Z. H.; Yang, T. X.; Yang, X.; Shi, W. H. Experimental study of non-linear water flow through unconsolidated porous media under condition of high hydraulic gradient. *Rock Soil Mech.* **2018**, *39*, 4017–4024.

(59) Zhang, L.; Tian, M. M.; Xue, J. H.; Li, M. X.; Zhang, C.; Lu, S. Effect of liquid nitrogen cycle treatment on seepage characteristics of coal samples with different water contents. *J. China Coal Soc.* **2021**, *46*, 291–301.